Investigation of Flowfields in Small Sonic Venturi-Nozzles

E. von Lavante [1], *M. Ishibashi* [2] *and G. Wendt* [3]
[1] *University of Essen, Germany*
[2] *NRLM, Japan*
[3] *PTB, Germany*

Abstract: Detailed investigation of flow fields associated with several sonic Venturi nozzles with small Reynolds numbers used for flow metering was carried out. The range of Reynolds numbers considered in this work extended from $4 \cdot 10^3$ *to* $4.4 \cdot 10^4$*. In the experimental part, global parameters such as discharge coefficient* C_d *and local flow variables such as recovery temperature* T_r *were investigated independently at two different scientific institutions. Both discovered flow phenomena that were not explainable using simple linear theories. Therefore, in the numerical part of the present investigation, the corresponding flow fields were simulated using compressible viscous flow solver ACHIEVE. The qualitative agreement of the numerical and experimental results was satisfactory; the comparison enabled the authors to explain most of the physical phenomena observed.*

Keywords: Critical Nozzles, Discharge Coefficient, Numerical Simulation

1 Introduction

The use of sonic nozzles in metrology is regulated by the still valid standard ISO 9300 [1]. Accordingly, the validity range of the corresponding measurement is limited to Reynolds numbers between 10^5 and 10^7. Many times, however, it is desirable to use nozzles at much smaller Reynolds numbers, either for applications with very small volumetric flows resulting in very small throat diameters, or for metering gases at very small pressures. In these cases, several investigators [3] [4] [5] [9] have discovered flow effects that were not consistant with the simple quasi-one-dimensional theory. These included variation of the discharge coefficient C_d as a function of the nozzle back pressure, not explainable by the theory offered in ISO 9300 [1], occurance of instabilities and pressure waves traveling upstream all the way through the throat and thus unchoking the nozzle for a very brief period of time, and the so called premature unchoking. In view of the above "horror" list, the present authors would like to stress that these phenomena do not effect reliable operation of the small sonic nozzle in any negative way, since they are consistant. After calibration, the corresponding nozzles still offer the same very reliable means of gas metering, as long as they are employed within their specifications.

The study of the above effects was difficult since, until recently, experimental methods used here were only capable of investigating global flow-rate dependencies, without being able to take a closer look at the details of the flowfield under investigation. On the other hand, all is not lost; small sonic Venturi nozzles still possess the same basic advantages of their larger counterparts. They represent a robust, consistent, simple and reliable means of metering gases and, after proper calibration, are highly accurate.

The good experience made by present authors as well as many other investigators with small sonic nozzles when employed in metrology to meter small mass flows justified further study of the corresponding flow fields in a hope to gain more detailed knowledge of their behavior. This, in turn, should make an explanation of most of the unusual effects occuring in these configurations possible.

With this motivation in mind, the present authors undertook an experimental and numerical investigation of air flow in sonic nozzles characterized by small Reynolds numbers. A special feature of the present work is the close cooperation between the experimental and numerical parts of this study.

2 Numerical Algorithm

The numerical method employed in the present flow simulations is part of a flow simulation system developed at the Institute of Turbomachinery at the University of Essen, called "ACHIEVE". It consists of an upwind solver of the Navier-Stokes equations, using the finite volume discretization. The governing equations to be solved in the present simulations are the two-dimensional or axisymmetric compressible Navier-Stokes equations. The governing equations are given in more detail by, for example, Steger [7] or von Lavante et. al. [6].

2.1 Numerical Scheme

Due to the complexity of the predicted flow, a simple numerical scheme with central spacial differences and artificial dissipation added explicitely was not suited for the present simulations. Therefore, the well known and proven Roe's Scheme [2] was employed. The numerical scheme is based on Roe's Flux Difference Splitting in finite volume form, as developed by von Lavante et. al. [6]. The method has been proven to be accurate and effective in the simulation of viscous flows with wide range of Mach numbers [2].

The simulations were carried out on structured grids. The mesh points were arranged according to an algebraic distribution and clustered at the solid walls to ensure enough gridpoints in the boundary layers. The domain was divided into several blocks to make the formulation of the boundary conditions and handling a complex geometry easier. Furthermore, the Multiblock-structure was necessary to compute the flow on parallel computers.

The present numerical scheme is described in more detail in a companion paper by von Lavante et al. [13] in these proceedings; more comprehensive information about the numerical and mathematical aspects of the present algorithm is offerred in [14].

2.2 Discretization in Time

The governing equations were integrated in time by solving their semidiscrete form by means of either modified Runge-Kutta (R-K) time stepping or implicit symmetric Gauß-Seidel (SGS) relaxation method. In the present work, the two stage version of the R-K procedure was utilized. The corresponding Runge-Kutta coefficients α_i were optimized by von Lavante et al. [8] for maximum multigrid performance (damping of high frequencies). That optimization was done, however, using a linear hyperbolic model equations. In realistic applications, these coefficients worked fine for the inviscid Euler equations as well as for most viscous cases. The simple two stage R-K procedure was as efficient as the more frequently used four stage scheme, but required only one optimized coefficient, $\alpha_1 = 0.42$.

2.3 Boundary Conditions

The present boundary conditions were implemented with the help of dummy (ghost) cells. At the subsonic inflow boundary, a locally one-dimensional weakly non-reflective boundary condition, based on the isentropic theory of the Riemann problem, was used. The tangential velocity, incoming Riemann invariant, total pressure and entropy in the first ghost cell were specified. The outgoing Riemann invariant was extrapolated from the interior domain. At the subsonic outflow boundary, the static pressure was specified, subject to the fluctuations allowed by the non-reflective treatment. The remaining variables were extrapolated. At solid walls, the velocities were anti-reflected, resulting in zero velocity on the boundary. The static pressure and density were reflected, resulting in zero gradients of these variables at the wall (adiabatic wall). Finally, at the interzonal boundaries, the block grids were overlapping by two cells, providing smooth transitions of the dependant variables

Q due to the present MUSCL extrapolation in the projection phase.

3 Experimental Methods

The experimental part of the present research work has been done in two different laboratory facilities and will be, therefore, described for each laboratory separately.

3.1 Experimental setup at the PTB

The present research efforts concentrate on flow behavior in sonic nozzles with small Reynolds numbers between $1.7 \cdot 10^3$ and approximately $5 \cdot 10^4$; therefore, only investigations done at the PTB with nozzles of sizes up to 2 mm throat diameter and volumetric flow rates between 0.01 and 2.2 m^3/h will be considered here. In order to measure the massflow rates and the corresponding C_d coefficient accurately and reliably, the primary volume and flow rate standards of PTB were used. In the present case, one of the two piston devices [10] available for measuring small flow rates were employed in the appropriate range. The resulting overall expanded uncertainties were less than 0.12%. Details of this installation are given in a companion publication by Wendt and von Lavante [11] and will not be repeated here.

The nozzles investigated by the third author at the PTB were manufactured in sizes 0.15, 0.20, 0.25, 0.30, 0.40, 0.50, 0.60, 0.80, 1.0 and 2.0 mm, given for the throat diameter D^*. They were all geometrically similar and followed the guidlines set by the ISO 9300 standard. The corresponding shape can be seen in Fig. 6, displayed together with the computational grid. They had a toroidal shape with a diffuser of $7D^*$ length and 3.5 degrees diffusion angle. The working fluid was air at atmospheric conditions; the various Reynolds numbers were achieved by using nozzles of different size.

3.2 Experimental setup at the NRLM

The NRML laboratory has a wide variety of experimental equipment to investigate flows in metrological configurations at its disposal. Here, only the apparatus immediately associated with the present work will be discribed.

The nozzle under investigation, shown in Fig. 1, had also a toroidal shape with a throat diameter of 13.4 mm. The nozzle is characterized by a relatively short diffuser, having a total length of $4D^*$. The diffuser opening angle was 3 degrees. A unique serial connection of two critical nozzles was used to facilitate monitoring the C^d coefficient of the test nozzle (second in streamwise direction). The working medium was air, entering the first (reference) nozzle at atmospheric pressure, room temperature and ambient humidity. A vacuum pump was arranged behind the second (test) nozzle, while the first nozzle served as a reference device. Different Reynolds numbers were accomplished by changing the total pressure ahead of the second (test) nozzle. The entire experimental setup is described in [12].

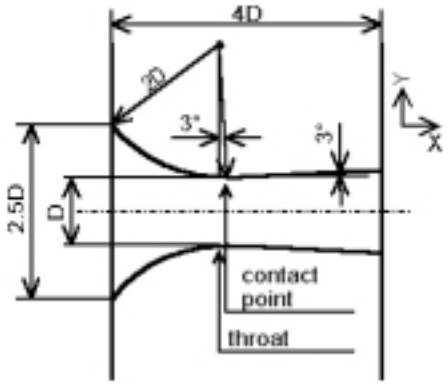

Figure 1. Cross-section of the nozzle used in the NRLM experiments.

It was deemed by the authors that the physical phenomena listed above could be reasonably explained only if detailed flow field information obtained by experimental und numerical methods was available. Until recently, however, there were no reliable nonintrusive methods to provide an information about the corresponding flow fields in sufficient detail. Fortunately, the second author of the present paper developed a procedure to measure the so-called recovery temperature that produces essentially no disturbance to the flow field in the nozzle. He deviced a traverse system (Fig.2) consisting of an axially arranged thermocouple. The lead wires are made of Alumel and Chromel, respectively, supported by slender tubes of elliptical cross-section. The temperature was measured directly by a multimeter using its thermocouple function. The contact point, shown in Fig.2, could by linearly translated in the axial direction (x-axis) or rotated about the x-axis, allowing access to any point within the nozzle. The stagnation temperature was selected as the reference temperature and was obtained by moving the contact point all the way upstream. The origin was found by first moving to the inlet plane of the nozzle while monitored by a telescope, and then substracting the known length from the inlet plane to the throat. This procedure was possible since the nozzle was manufactured by a super-accurate lathe [12].

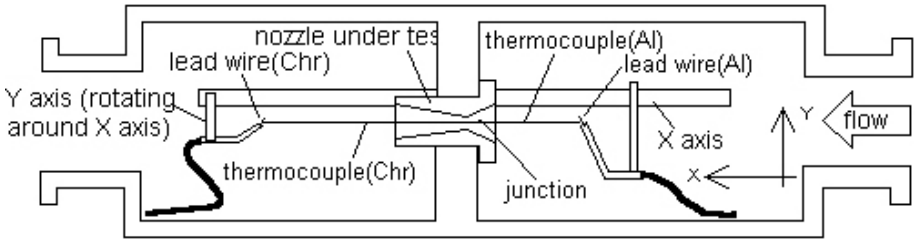

Figure 2. Arrangement of the thermocouple device.

4 Discussion of Results: Global View

In this chapter, results obtained by the third author for the discharge coefficient C_d and volumetric flow rates in geometrically similar nozzles of different size will be introduced and discussed. Main emphasis is put on the dependency of the critical outlet (back) pressure ratio $(p_{out}/p_0)_{crit}$ on the nozzle Reynolds number as defined by the ISO 9300. In these experiments, the outlet pressure ratio p_{out}/p_0 was first set to a low value, typically 0.04, at which the flow in the throat certainly was critical, and the massflow therefore remained constant. The outflow pressure was then gradually increased. The present so-called PTB-nozzles, shown in Fig. 6, had an area ratio $A_{out}/A^* = 3.42$. According to a simple quasi-one-dimensional theory presented in the ISO 9300 [1], the flow in the throat will just unchoke when the back pressure ratio reaches approximately $p_{out}/p_0 = 0.89$. At this point, the massflow will start decreasing from its maximum value. The critical back pressure ratio was, therefore, defined as the back pressure ratio p_{out}/p_0, at which the flow rate just dropped by 0.05%.

Experiments done with nozzles with throat diameters between 0.15 and 2.0 mm revealed, however, that the critical back pressure ratio was much lower than the theoretical value. The resulting plot of the normalized flow rate as a function of p_{out}/p_0 for various nozzles is presented in Fig.3. Even for the largest nozzle in the picture ($d^* = 1.0\ mm,\ Re_{ISO} = 1.1 \cdot 10^4$), the critical back pressure ratio was at 0.69 much smaller than the theoretical value of 0.89. The smallest nozzle tested ($d^* = 0.15\ mm,\ Re_{ISO} = 1.7 - 1.9 \cdot 10^3$) had a critical pressure ratio of 0.46, which was, surprisingly, smaller than the critical pressure ratio for air, $p^*/p_0 = 0.528$. Using the definition of critical back pressure given above, its dependency on the throat diameter can be determined from Fig. 3. It is shown in Fig.4 for various nozzles from two sets, manufactured in 2 batches, respectively.

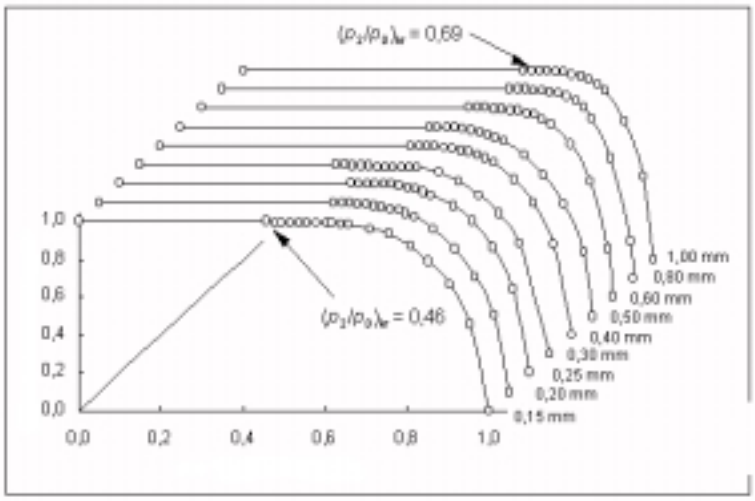

Figure 3. Normalized flow rate as a function of p_{out}/p_0 for nozzles of different size.

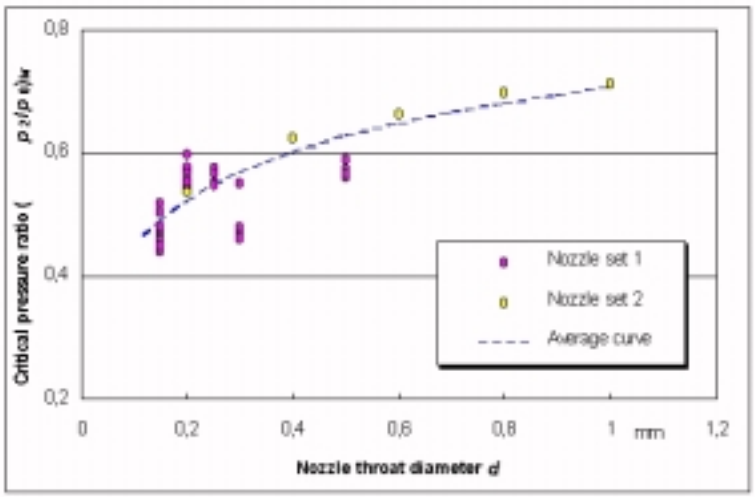

Figure 4. Critical back pressure ratio as a function of throat diameter d^*.

The critical back pressure for the nozzles from the set 2 decreases rapidly for throat diameters below approximately $d^* = 0.4\ mm$. On the other hand, as the throat diameter increases, it seems to approach slowly the theoretical value of 0.89. The critical back pressure for the nozzles from the set 1 display, unfortunately, no clear tendency. Generally, however, even in this case, the values for the critical back pressure are clustered around 0.5 and remain below 0.6. A curve-fit through the measured points can be seen as a dashed curve. Its validity for the small d^* is, however, questionable.

The above behavior of the critical back pressure is called "premature unchoking phenomenon" and has been discovered and investigated independently by, among others, Ishibashi et all [4] or Nakao [9]. It is strongly dependent on the Reynolds number and has been, therefore, suspected to be connected with mainly viscous effects. In order to compare the results in Fig. 4 with those of other investigators, the critical back pressure is expressed as a function of the Reynolds number Re_{ISO}, displayed in Fig.5.

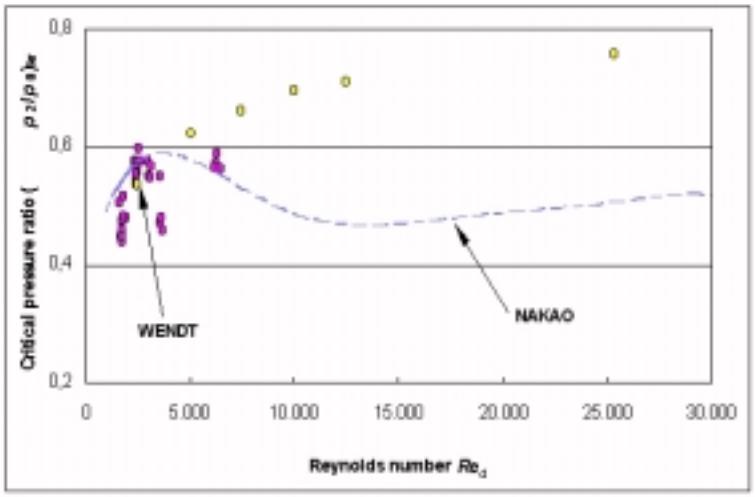

Figure 5. Critical back pressure ratio as a function of the Reynolds number Re_{ISO}.

In Fig.5, the results obtained at the PTB-Laboratory are compared with data published by Nakao [9]. Nakao investigated the critical back pressure for different gases and Reynolds numbers in a nozzle similar to the NRLM-nozzle displayed in Fig.1. Here, only his results for nitrogen were considered, judged comparable with air. At a first glance, there seems to be glaring discrepancy between the two data sets. At very low Reynolds numbers, $Re_{ISO} < 5 \cdot 10^3$, both results agree rather well. At Reynolds numbers above this value, however, the PTB-measured critical back pressure uniformly increases, whereas the NRLM results show first a slight increase, followed by a gentle decrease to approximately 0.5. Then, for a fairly extensive range of Reynolds numbers, the critical pressure according to Nakao remains nearly constant at 0.5. Eloquently, this pressure ratio was therefore called the "magic pressure ratio".

Some of the differences can be explained by noticing that the nozzle studied by Nakao featured a much shorter diffuser, having an area ratio of $A_{out}/A^* = 1.56$, resulting in theoretical critical back pressure ratio of approximately $p_{out}/p_0 = 0.81$. Still, the theoretical ratio of the critical back pressures would be only about 1.1, accounting only for some of the difference between the two results. As the significance of the viscous effects increases, the essentially inviscid theory looses its validity and both data sets approach each other. It was decided to simulate the corresponding flow field numerically in order to obtain further clues about the flow in question.

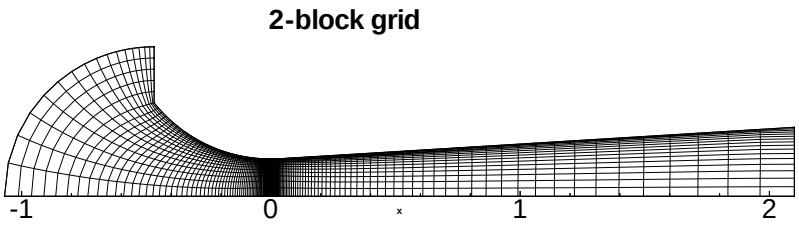

Figure 6. Computational grid for the PTB-nozzle.

Since the flow was assumed to be axially symmetric, the computational domain was limited to the upper half of the nozzle. Its shape including the computational grid is shown in Fig. 6. For clarity,

only every second line is shown axially, and only every fourth line is shown in direction normal to the wall. The flow enters the domain through the left boundary and exits downstream of the diffuser. Closer to the wall (upper boundary), the grid resolution is exponentially increased.
The flow in the PTB-nozzle was simulated for two Reynolds numbers, $3.7 \cdot 10^3$ and $1.0 \cdot 10^3$, corresponding to throat diameters of 0.3 mm and 0.1 mm, respectively. The resulting countours of constant density and velocity can be seen in Fig. 7 for the higher Reynolds number and in Fig. 8 for the lower Reynolds number.

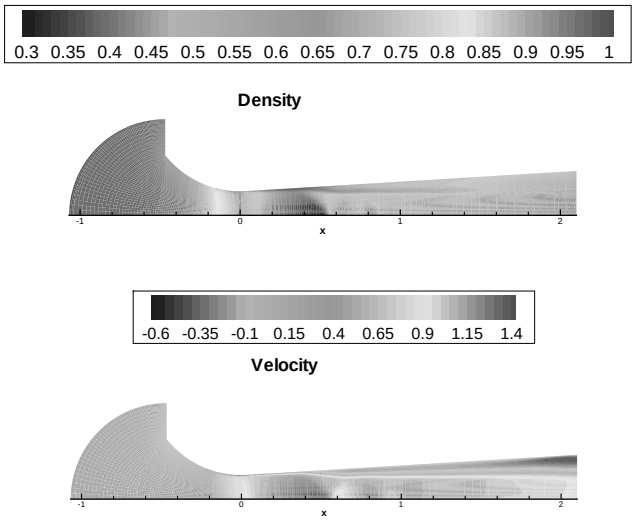

Figure 7. Resulting density and velocity contours for $Re_{ISO} = 3.7 \cdot 10^3$; $p_{out}/p_0 = 0.55$.

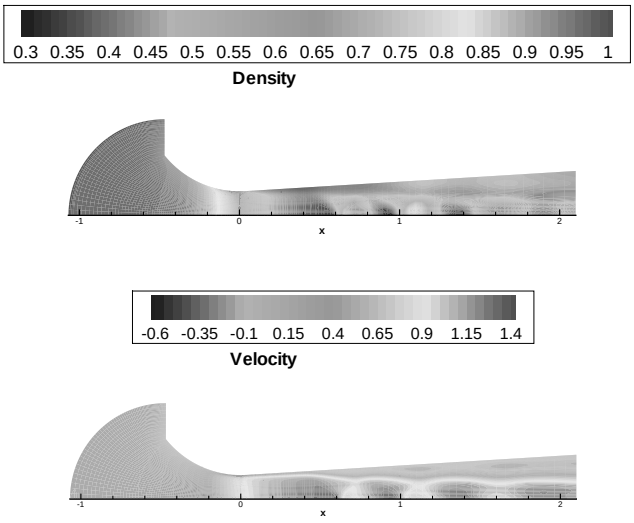

Figure 8. Resulting density and velocity contours for $Re_{ISO} = 1.0 \cdot 10^3$; $p_{out}/p_0 = 0.4$.

In the case of $Re_{ISO} = 3.7 \cdot 10^3$, corresponding to a real critical Reynolds number $Re^* = 4.3 \cdot 10^3$, the velocity contours reveal a massive separation of the boundary layer, starting almost immediately downstream of the throat. The flow field is divided into an essentially inviscid core flow and an almost equally extensive region of separated shear layer, dominated by viscous effects. In the case of approximately constant pressure along the diffuser, the core flow forms a stream-tube of approximately constant cross-sectional area surrounded by the conical (axisymmetric !!) viscous region. Slightly downstream of the throat, critical flow conditions are reached, with a local pressure ratio of $p/p_0 = p^*/p_0 = 0.528$. When the back pressure is maintained at levels close to the same pressure ratio (about 0.5), the core flow will experience very small pressure gradients and will be, therefore, basically disturbance free. In the case of slightly higher outflow pressure, positive pressure gradients will be imposed on the core flow, leading to the formation of shocks (Fig. 7). The shocks will apear as oblique shocks (x=0.5 mm, Fig. 7) that will become stronger and increasingly unsteady with increasing outflow pressure. The density contours (upper part of Fig. 7) also give an indication of the oblique shock and the very thick separated boundary layer. In the downstream part of the diffuser, the density gradients normal to the wall are becoming smaller due to mixing and dissipation. The pressure across the outflow plane is fairly uniform, assuming the specified value p_{out}/p_0. At back pressure ratios larger than approximately 0.6, unsteady pressure waves start travelling upstream, causing intermittent unchoking of the throat. The duration of the subcritical flow periods is only about $100\ \mu s$, making these waves hardly detectable. They will, however, result in a slight decrease of the average massflow and discharge coefficient C_d. Further moderate increase of the outflow pressure will have no significant effect on the flow, explaining the "plateau" in the C_d plot in Fig. 3. Finally, at still higher outflow pressure, the nozzle will completely unchoke (at all times), leading to a strong decrease of the flow rate.
The opposite situation can be seen in Fig. 8 for a Reynolds number $Re_{ISO} = 1 \cdot 10^3$. Here, the boundary layer is even thicker, and the back pressure ratio is 0.4, lower than the "magic pressure ratio". The core flow undergoes a series of overexpansions to supersonic Mach numbers, followed by stationary shocks. The flow is reminiscent of overexpanded free jets with a system of Mach-discs.

The flow, in particular in the boundary layer, is stable due to the favourable pressure gradient.

It is important to note that the boundary formed by the separated shear layer is much more sensitive to pressure gradients in the core flow than relatively thin attached boundary boundary layers found in the diffuser in case of larger Reynolds numbers. In the present case of nozzles with small Reynolds numbers, the classical diffuser design according to ISO 9300 [1] does not seem to be appropriate. Its shape, however, is still relevant, as noticed in Fig. 5. The longer diffuser in the PTB-nozzle makes better adjustment of the flow to the given back pressure possible, as demonstrated by the higher critical back pressure ratio.

5 Discussion of Results: Details of Flow Field

The recovery temperature measurements carried out at the NRLM offer detailed information about the flow field in the nozzle in Fig. 1 not available previously. The thermocouple used in the experiments discussed in this paper had a diameter of 13 μm. The main advantage of the present method is that it is essentially nonobstructive. It is assumed that the thermocouple, arranged as shown in Fig. 2, will indicate the recovery temperature at the contact point. After some simple manipulations [4], the difference between the recovery temperature and the stagnation temperature can be expressed as:

$$\Delta T_{r0} \;=\; T_{rec} \;-\; T_0 \;=\; -\left(1-\sqrt{Pr}\right)\cdot\frac{\kappa-1}{\kappa+1}\cdot T_0\cdot M^{*2} \qquad (1)$$

where Pr is the Prandtl number, assumed here to be 0.73. M^* is Mach number with the critical speed of sound taken as the reference. The same expression has been used in the present numerical simulations with a small twist. In view of the unsteady flow in parts of the nozzle, it should be realized that the recovery temperature measurements, performed at one location, represent a time-wise average over at least a few seconds. Therefore, the simulated recovery temperature had to be averaged over at least several cycles of the periodic flow motion.

In the present work, only the test case with total pressure $p_0 \;=\; 26\ kPa$ and total temperature $T_0 \;=\; 298.15\ K$, resulting in a Reynolds number $Re_{ISO} \;=\; 4.4\cdot 10^4$, was considered. The resulting recovery temperature difference as measured at the NRLM is presented below in Fig. 9. The same results shown as a carpet plot of the absolute value of the recovery temperature difference for the lowest back pressure ratio of 0.3, displayed over a cross-section of the nozzle, can be seen in Fig. 10. These can be compared with the results of the present numerical simulation in Fig. 11. The flow in the throat is critical and steady. However, contrary to the inviscid theory, about 1.5 mm downstream of the throat (the origin of the x-axis) an oblique shock is visible in both pictures. The shock forms at a point of discontinuous second derivative of the wall shape, where the circular contour meets the conical diffuser. According to the viscous theory, the laminar boundary becomes thicker at this location, generating an oblique shock. The experimentally determined shock is at the same location but stronger than in the simulation. This is at first puzzling, but a closer look at its shape reveals that in Fig. 10 it is almost normal to the wall. This is typical of condensation shocks, which can form at humidities even below 50 % . In Fig. 14, the instantaneous density contours are compared to the averaged recovery temperature. The oblique shock discussed above is rather weak and therefore barely visible. At x=18 mm, the boundary layer separates due to the weak shock, producing a stronger oblique shock that becomes normal to the center line. This shock is not visible in Fig. 10, since the x-axis reaches only until 16 mm. This stronger shock is at the same position in both the instantaneous and averaged pictures, and is crisp and clearly defined by the recovery temperature contours. Therefore, it can be deduced that it is essentially stationary. The separated boundary layer can be also seen in both pictures. It is unsteady only after it leaves the nozzle.

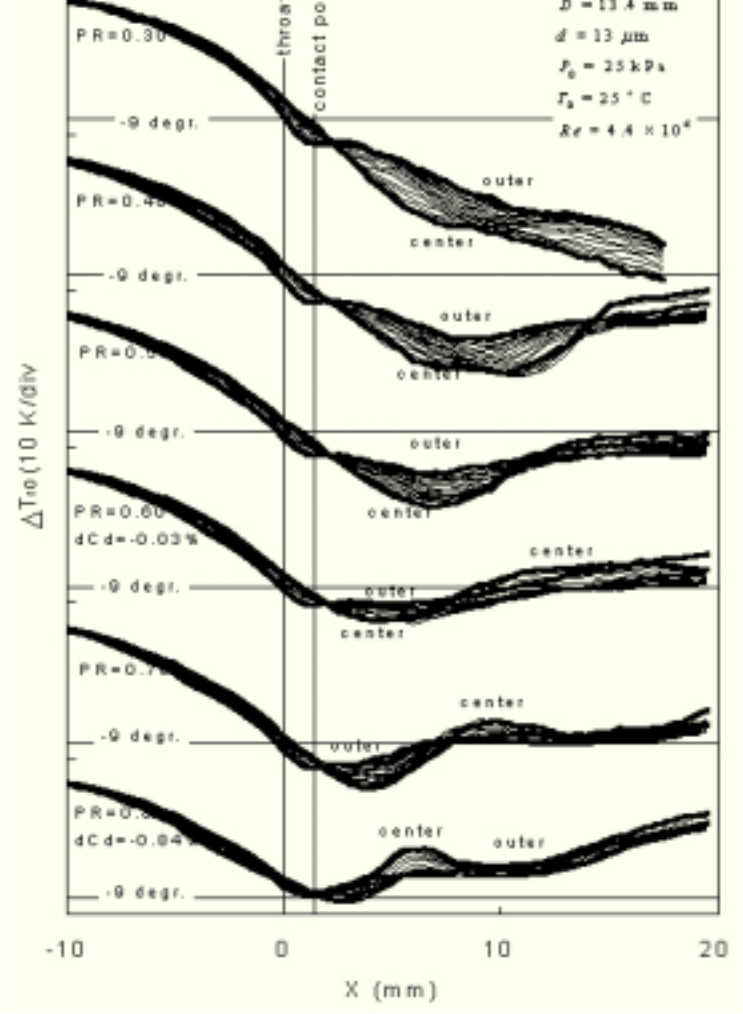

Figure 9. Recovery temperature difference along the nozzle for various outflow pressure ratios.

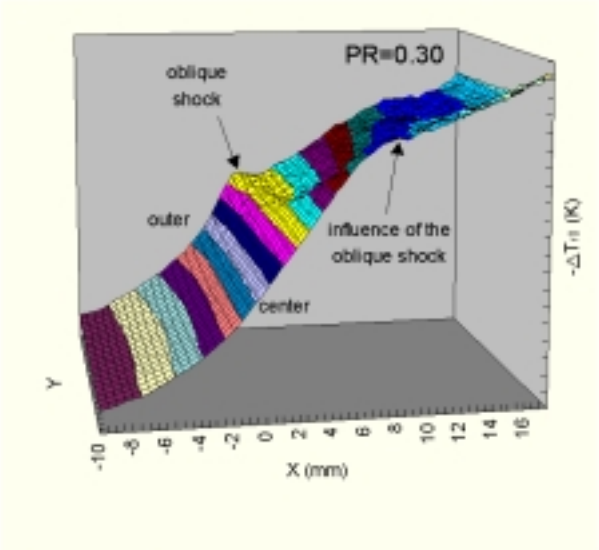

Figure 10. Measured absolute value of recovery temperature difference.

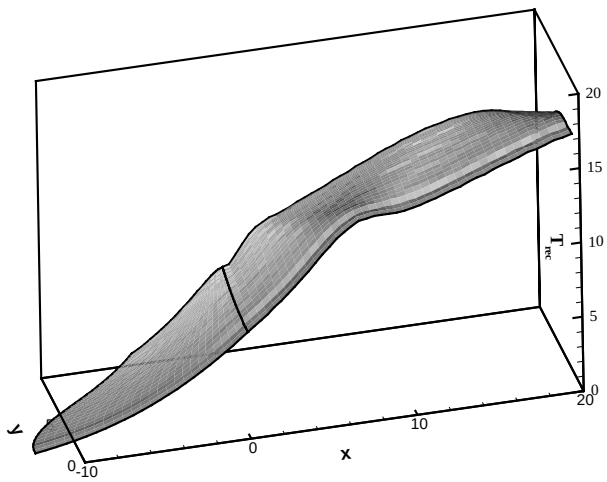

Figure 11. Computed absolute value of recovery temperature difference.

At a back pressure ratio of 0.4, the stronger shock moves forward, as seen in Fig. 9. The shock is still well defined and therefore probably stationary. After increasing the back pressure ratio to 0.5, the stronger shock coincides with the weaker leading (condensation) shock at x=7-8 mm. The

measured recovery temperature for this case is shown in Fig. 12; the simulated one in Fig. 13. The corresponding flow field can be seen in Fig. 15. Here, in both time-averaged pictures (experiment and simulation), the shock is not well defined, indicating that it is moving along the nozzle, smearing its image. In the simulation, fairly weak pressure were traveling upstream, very briefly unchoking the throat. This coincides with a slight decrease of the measured C_d coefficient. The instantaneous density countours in Fig. 15 indicate a lambda-shock in the nozzle as well as the already discussed oblique shock. In the time-averaged picture of the recovery temperature, only the later shock can be clearly seen, indicating that it is still stationary. The second strong shock can not be distinguished, but the recovery temperature is nearly constant in the experiment and the simulation. Thus, it can be assumed that the second shock is unsteady, becoming more normal and therefore stronger as it moves toward the throat. The thick separated boundary layer can be seen in Fig. 13 and 15 as a region of higher (lower absolute value) recovery temperature in the upper rear corner.

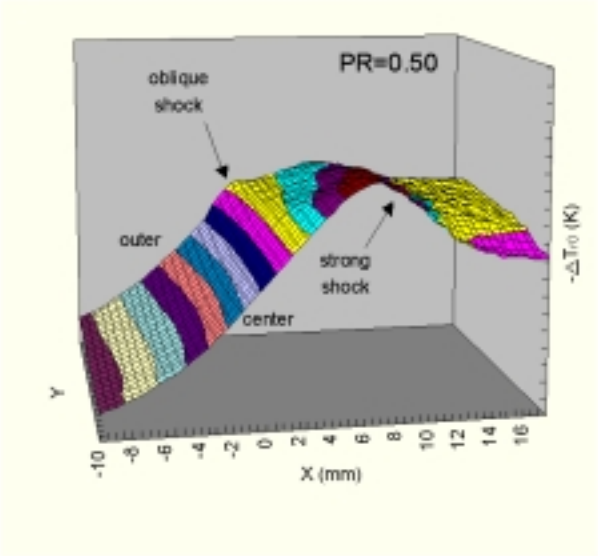

Figure 12. Measured absolute value of recovery temperature difference.

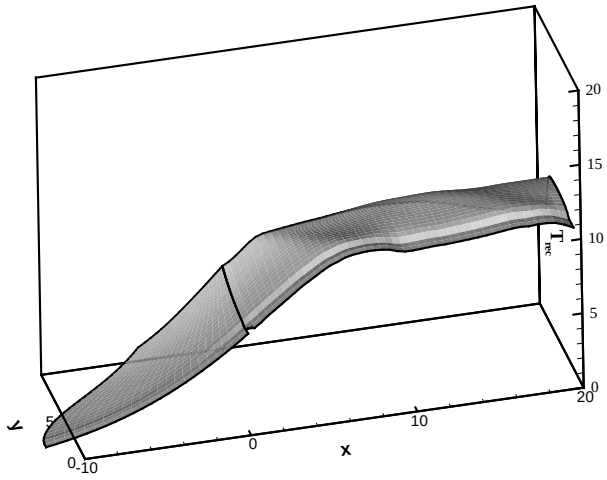

Figure 13. Computed absolute value of recovery temperature difference.

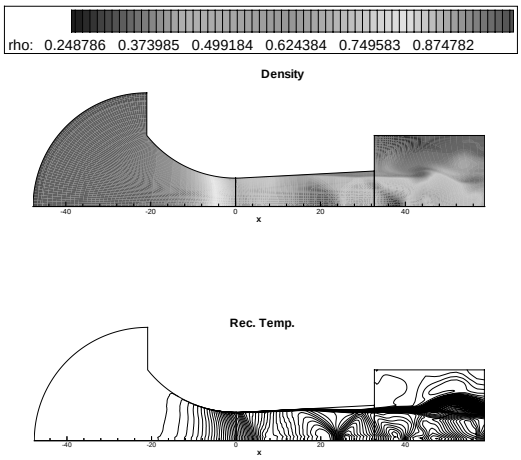

Figure 14. Instantaneous density and averaged recovery temperature contours, $p_{out}/p_0 = 0.3$.

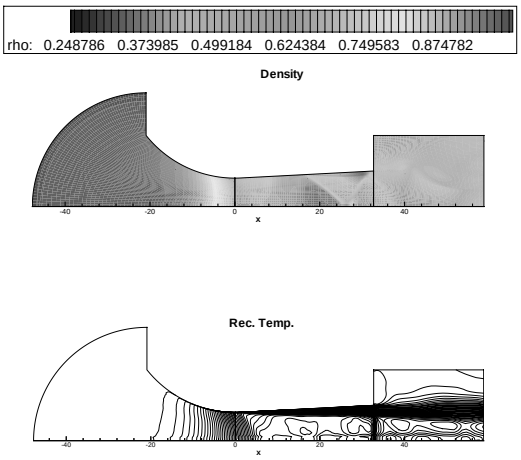

Figure 15. Instantaneous density and averaged recovery temperature contours $p_{out}/p_0 = 0.5$.

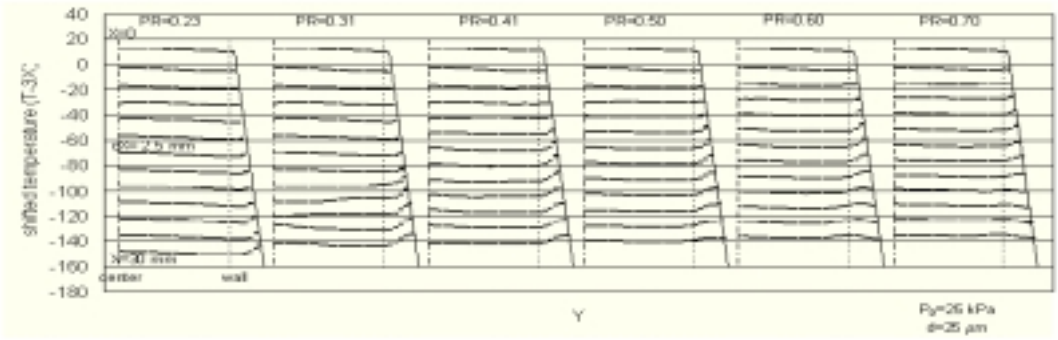

Figure 16. Recovery temperature measured by an inclined wire for various outflow pressure ratios.

The arrangement of the thermocouple wire parallel to the x-axis offered essentially zero flow disturbance, but was not able to investigate the flow in the boundary layer. Hence, a wire inclined by 3.0 degrees parallel to the diffuser wall was used to reach into the viscous region. In this case, the thermocouple had a diameter of $25\ \mu m$. The resulting recovery temperature is displayed in Fig. 16. The measured curves were shifted by $T_{plot} = T_{rec} - 3 \cdot x$ in order to compare the results at different axial stations. The data in Fig. 16 confirm the simulation results and the consequent hypothesis regarding the flow behavior.
At the smallest back pressure ratio of 0.23 (not simulated), the core flow has to accelarate in order to decrease the local pressure ratio from 0.528 to 0.23. Therefore, the cross-section of the core increases. The boundary layer is stabilized by the favourable pressure gradient, is relatively thin and probably attached.
In excellent agreement with the simulation, the boundary layer in the case of $p_{out}/p_0 = 0.31$ separates at approximately x=15 mm, becoming thicker. The core flow stream-tube has an almost constant cross- sectional area.
At $p_{out}/p_0 = 0.5$, the boundary layer is separated almost all the way from the throat. The cross-section of the core region actually decreases. The flow in the separated boundary layer is beeng mixed out, resulting in a more uniform recovery temperature profile across the end of the diffuser. The same tendency can be seen in the following cases $p_{out}/p_0 = 0.6$ and $p_{out}/p_0 = 0.7$. The boundary layer becomes even thicker, the mixing is more intensive, the inviscid core smaller and slower.

3 Conclusions

Based on experimental and numerical investigations carried out with nozzles characterized by small Reynolds numbers, the authors were able to conclusively show that most of the unusual phenomena occuring in these nozzles are due to dominating viscous effects and their strong coupling with the core flow. The flow does not follow the diffuser contours, making its shape almost irrelevant. Clearly, a new approach for the design of small sonic Venturi nozzles is needed. However, once the proper back pressure ratio for fully choked operation is reached, the nozzles worked very reliably and accurately as flow metering devices.

The agreement between the experimental and numerical results was qualitatively very good; they complemented each other and were both essential in drawing the present conclusions.

[1] International Standard ISO 9300, "Measurement of gas flow by means of critical flow Venturi nozzles", First Edition, Beuth, Berlin 1990.

[2] von Lavante, E. and Grönner, J., "Semiimplicit Schemes for Solving the Navier-Stokes Equations", 9th GAMM Conference, Lausanne, Notes on Numerical Fluid Mechanics, Vieweg, 1992.

[3] von Lavante, E., Nath, B. and Dietrich, H., "Effects of Instabilities on Flow Rates in Small Sonic Nozzles", Proceedings of the 9th Int. Conference on Flow Measurement FLOMEKO'98, Lund, 1998.

[4] Ishibashi, M., von Lavante, E. and Takamoto, M., "Quasi- Nonintrusive Measurement of Flow Velocity Field in a Critical Nozzle", Proceedings of ASME FEDSM'00, June 11-15, Boston, 2000.

[5] Wendt, G., Ph.D. Thesis, University of Essen, Germany, 2000.

[6] von Lavante, E., El-Milligui, A. and Warda, H., "Simulation of Unsteady Flows Using Personal Computers", The 3rd Int. Congress on Fluid Mechanics, Cairo, 1990.

[7] Steger, J. L., "Implicit, Finite-Difference Simulation of Flow about Arbitrary Geometries", AIAA Journal, Vol. 16, No. 7, 1978.

[8] von Lavante, E., El-Miligui, A., Cannizzaro, F. E., and Warda, H. A., "Simple Explicit Upwind Schemes for Solving Compressible Flows", Proceedings of the 8th GAMM Conference on Numerical Methods in Fluid Mechanics, Delft, 1990.

[9] Nakao, Shin-ichi, "Choking Phenomenon of Sonic Venturi Nozzles on Low Reynolds Numbers", Proceedings of the 9th Int. Conference on Flow Measurement FLOMEKO'98, Lund, 1998.

[10] Aschenbrenner, A., "Kolbengeräte und Rohrprüfstrecken für die Prüfung von Volumengaszählern", DVGW-Schriftenreihe Gas/Wasser 12, pp. 113-134, 1987.

[11] Wendt, G. and von Lavante, E., "Influence of Surface Roughness on the Flow Rate Behavior of Small Critical Venturi Nozzles", Proceedings of the 10th Int. Conference on Flow Measurement FLOMEKO'2000, Salvador, 2000.

[12] Ishibashi, M. and Takamoto, M., "Very Accurate Analytical Calculation of the Discharge Coefficient of Critical Venturi Nozzles with Laminar Boundary Layer", Proceedings of the FLUCOME97, Hayama, Japan, Sept. 1997.

[13] von Lavante, E., Zachcial, A., Zeitz, D., Nath, B. and Dietrich, H., "Effects of Various Geometric Parameters on the Flow Behavior in Sonic Nozzles", Proceedings of the 10th Int. Conference on Flow Measurement FLOMEKO'2000, Salvador, 2000.

[14] von Lavante, E., Zachcial, A., Färber, J., Nath, B. and Dietrich, H., "Simulation of Unsteady Effects in Sonic Nozzles Used for Flow Metering", Proceedings of the 8th Int. Symposium on Computational Fluid Dynamics, Bremen, Sept. 1999.

AUTHOR(S): Prof. Dr.-Ing. Ernst von Lavante, Institute of Turbomachinery, University of Essen, 45127 Essen, Germany. E-mail: erni@tigger.turbo.uni-essen.de.
Dr. Masahiro Ishibashi, Mechanical Metrology Dept., Nat. Res. Lab. of Metrology, Tsukuba, Ibaraki, 305-8563, Japan. E-mail: ishi@nrlm.go.jp.
Dipl. Phys. Gudrun Wendt, Physikalisch-Technische Bundesanstalt, Postfach 33 45, 38023 Braunschweig, Germany. E-mail: Gudrun.Wendt@PTB.de.